Journal of The Electrochemical Society, **158** (1) D15-D20 (2011)
0013-4651/2010/158(1)/D15/6/$28.00 © The Electrochemical Society

Fabrication of a Gold Island Film on Porous Polymeric Substrates by a Strategic Electroless Deposition

Jeong Hoon Byeon[a] **and Jang-Woo Kim**[b,z]

[a]*Samsung Electronics Company, Limited, LCD Division, Yongin 446-711, Republic of Korea*
[b]*Department of Digital Display Engineering, Hoseo University, Asan 336-795, Republic of Korea*

This paper describes a new strategy for fabricating a gold (Au) island film based on a silver (Ag) aerosol surface activation onto a porous polytetrafluoroethylene (PTFE) substrate, followed by electroless deposition (ELD). Spark produced Ag aerosol nanoparticles (~12.3 nm in diameter) were physically captured (8.7 μg Ag/cm^2 PTFE in activation intensity) onto the surface of the substrate. After annealing (240°C) in nitrogen atmosphere, the activated substrate was placed into a solution for Au ELD (at 90°C). Successive Au deposition introduced an island film having the thickness of ~3.1 μm (the lateral dimensional and mass growth rates of 17.2 nm/min and 9.2 μg Au/cm^2 PTFE-min, respectively), which was similar to the diameter of the island films at 180 min of deposition. X-ray diffraction certified the uniformity of the films with the Au (111) crystallographic orientation as the predominant one. The corresponding crystallite sizes ranged from 14 to 62 nm for 60–180 min of deposition. Island Au growth was also achieved using the present method for a different porous substrate (polyamide). Through these results, the Ag aerosol activation on a substrate with an uneven surface structure might preferably introduce an island electroless growth of the Au.
 [DOI: 10.1149/1.3511776]

Manuscript submitted August 17, 2010; revised manuscript received October 15, 2010. Published November 19, 2010.

The unique physical properties of gold (Au) fine particles, whether involving single particle ensembles or films, continue to interest a variety of scientists and engineers.[1] Au film/substrate structured materials have been widely exploited for use in selective chemical syntheses,[2] catalytic eliminations of environmental pollutants,[3] biological applications,[4] in situ polymerizations,[5] and optoelectronic applications.[6] In particular, Au island films on substrates[7-11] are interesting systems manifesting electron and light emissions as well as nonlinear, and sometimes nonmonotonic, conduction current-voltage curves.[12] Regarding the Au metallization of a substrate, there are several possible approaches including vacuum evaporation-deposition-sputtering, electrochemical, and electroless deposition (ELD) methods.[13] Methods such as evaporation or sputtering present good alternatives for Au metallization on substrates, but they are expensive to operate and need specialized conditions for uniform Au deposition on the desired surface. The ELD technique enables metallic Au films easily and uniformly to deposit on the surfaces even with complex configurations,[14] without an external electric current, via oxidation-reduction reactions.[15] As a starting point for developing methodologies, several groups have carried out ELD of Au on a variety of substrates and by a variety of methodologies.[16-18] Martin and co-workers[19-21] have successfully applied ELD techniques to the Au particles and tubes in templates by the chemical reduction of a commercial Au ELD solution by formaldehyde.

Recent attention has been given to Au ELD by galvanic displacement of less noble metals by Au,[13,19-28] focusing on the deposition of the Au structures such as island (discontinuous) and land (continuous) thin films. The procedure used for Au ELD consists of several steps. First, tin ion (Sn^{2+}) must be adsorbed onto the deposition surface which is then immersed in an aqueous solution of ammoniacal silver nitrate so that the surface becomes coated with nanoscopic silver (Ag) particles. The Ag activated substrate is immersed in a Au ELD solution for several hours to achieve a good deposition. In this step, the Ag particles are galvanically displaced by Au because Au is a more noble metal, and the resulting Au particles are excellent sites for the oxidation of reducing agents and the concurrent reduction of Au ions to Au atoms.[29] Finally, the Au deposited substrate is immersed in nitric acid to dissolve residual Sn that might be strongly adsorbed on the surface. Even though a cheap Ag activation could be performed on Au ELD, it was still necessary to use wet chemical steps for the activation and post-treatment which might create environmental pollution problems and could need expensive and time-consuming recycling processes and thus methods to avoid their use should be pursued.

There are some reports on ELD of Au using Au(I) cyanide compounds[18,30,31] for the reason that Au(I) cyanide is stable in an alkali solution and is easily obtained. But cyanide compounds have a heavy toxicity;[32] thus, they are not convenient in experiments and do great harm to the environment. Recently, Jing et al.[33] used the complex ions of $[AuCl_4]^-$ as the main salt for Au ELD. Compared with other cyano complexes of Au (i.e., sodium gold cyanide, potassium gold cyanide, and ammonium gold cyanide), $[AuCl_4]^-$ has little toxicity, so it is safer to the environment.[33] The ELD solution containing $[AuCl_4]^-$ is more stable when a stabilizer (ethylenediamine) is added and the *p*H range is 9.0–9.5.

In this study, a fabrication of the Au island films on porous polymeric substrates [polytetrafluoroethylene (PTFE) and polyamide (PA)] with a novel activation process was developed. Aerosol activation[34-36] using Ag nanoparticles was used to catalytically activate each of the substrates in a simple manner, and thus to introduce metallic Ag sites onto the substrate surface for Au ELD. A subsequent noncyanide Au ELD was introduced to generate Au island films by the galvanic displacement and autocatalysis during the deposition in an environmentally friendly manner.

Experimental

Our catalytic surface activation (Fig. 1a) involved the spark production of Ag aerosol nanoparticles and their capture by commercial porous polymeric substrates (47 mm in diameter and 0.2 μm in pore size, 11807-47-N for PTFE and 25007-047 N for PA, Sartorius, Goettingen, Germany). The porous substrates were used to enhance the formation of the Au island films as well. A spark was formed between two identical Ag rods (diameter: 3 mm, length: 100 mm, Nilaco, Tokyo, Japan) inside a reactor under a pure nitrogen environment at standard temperature and pressure.[37] The spark discharge is a kind of atmospheric nonequilibrium plasmas.[38] While the collision rate of electrons, ions, and neutrals is high, the discharge does not reach thermal equilibrium because it is short-lived, being interrupted before an arc discharge.[39] The flow rate of the nitrogen gas, which was controlled by a mass flow controller, was set to 6 l/min. The electrical circuit specifications were as follows: resistance of 0.5 M Ω, capacitance of 10 nF, loading current of 3.0 mA, applied voltage of 3.6 kV, and a frequency of 860 Hz. For reference, metal nanoparticles can also be produced at rates of several milligrams per hour by an arc discharge under high power, about 1 kW (several tens of amperes at several volts).[40] Thus, the arc method occasion-

[z] E-mail: jwkim@hoseo.edu

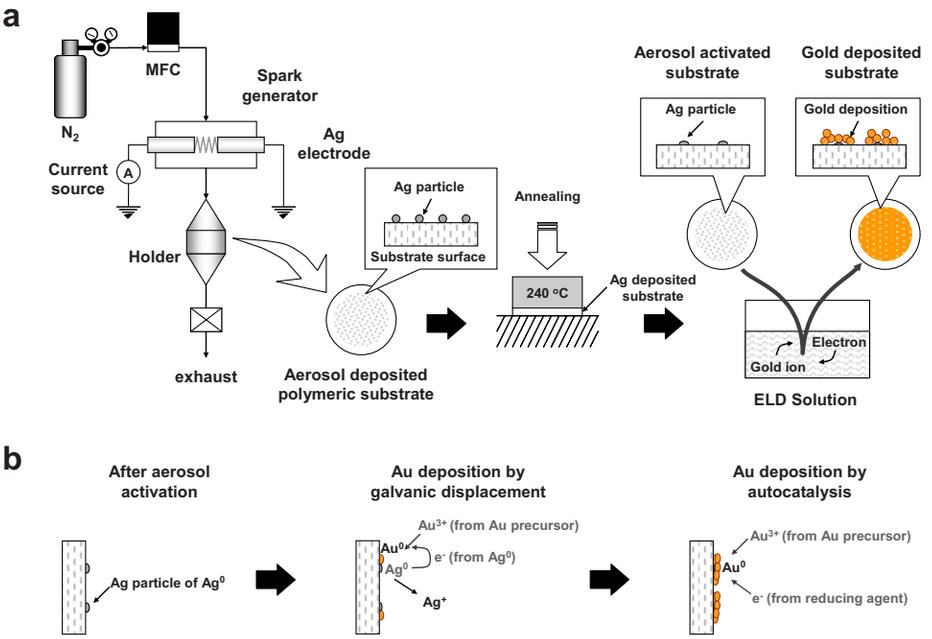

Figure 1. (Color online) (a) Diagram of the experimental procedure. (b) Scheme of the Ag aerosol activation and Au ELD.

ally induces a large proportion of unwanted products (e.g., large agglomerates) due to the harsh production condition arising from the high energy generated during the process.[41] In order to prevent the detachment of the nanoparticles from the surface of the substrates, the substrates were separated from the holder and annealed in nitrogen gas at 240°C (PTFE) and 160°C (PA) for 10 min after separation. Once the substrates were activated by the aerosol surface activation, the substrates were immersed (Fig. 1a) in ELD solutions (80 mL) for the deposition of Au onto the surface of the activated substrates. The bath temperature was maintained at 80°C. The substrates were vigorously rinsed with Milli-Q water (Millipore 18.2 M Ω cm^{-1}) after the ELD to remove the residual and then set aside to be dried.

0.025 mol/l $[AuCl_4]^-$ stock solution was prepared by dissolving 0.1 g Au (99.99%) in 10 mL concentrated nitro-hydrochloric acid in a temperature controlled water bath at 95°C. The corresponding dissolving reaction is as follows[33]

$$Au + 4HCl + HNO_3 \rightarrow HAuCl_4 + NO + 2H_2O \quad [1]$$

Then 0.1 g KCl and 40 mL HCl (36%) were added. The solution was finally diluted to 100 mL with chlorine-saturated water. The composition of the Au ELD solution was 0.025 mol/l $[AuCl_4]^-$ (stock solution), 0.05 mol/l NaH_2PO_2 (reducing agent), and 0.3 mol/l $NH_2CH_2CH_2NH_2$ (stabilizer), which was a slight modification of that reported by Jing et al.[33] KOH was used to adjust the *p*H ($\sim$9) of the solution. In Fig. 1b, Ag aerosol activation produced a seed layer on the substrate surface and followed Au deposition on the Ag sites. The Au ELD step, referred to as displacement deposition, consisted of replacing the Ag on the substrate surface with Au. Since Au is a more noble metal than Ag, the Au^{3+} ions will displace the Ag on the surface, leaving Au and returning the Ag^+ to solution,[9,25] and the reaction is as follows

$$Au(III)_{aq} + 3Ag(0)_{surf} \rightarrow Au(0)_{surf} + 3Ag(I)_{aq} \quad [2]$$

(The subscripts aq and surf denote species dissolved in solution and species attached to the substrate surface, respectively.) These surface-bound Au particles are autocatalysts for the reduction of Au(III) to Au(0) using NaH_2PO_2 as the reducing agent. For the autocatalytic deposition of Au, the following electrochemical reactions are considered[33]

$$AuCl_4^- + 3e \rightarrow Au + 4Cl^- \ (E^o = 1.00\ V) \quad [3]$$

$$HPO_3^{2-} + 2H_2O + 2e \rightarrow H_2PO_2^- + 3OH^- \ (E^o = -1.65\ V) \quad [4]$$

where E^o is the standard reduction potential. Therefore, we could infer that the redox reaction between $AuCl_4^-$ and $H_2PO_2^-$, as indicated in Reaction 5 below, is thermodynamically possible by comparing its E^o value to that of Reactions 3 and 4. The electrons required for the Au deposition are supplied by the oxidation of $H_2PO_2^-$

$$2AuCl_4^- + 3H_2PO_2^- + 9OH^- \rightarrow 2Au + 8Cl^- + 3HPO_3^{2-} + 6H_2O \quad [5]$$

The size distribution of the Ag aerosol nanoparticles was measured using a scanning mobility particle sizer (SMPS) consisting of an electrostatic classifier (3085, TSI, MN, US), ultrafine condensation particle counter (3025, TSI, MN, US), and aerosol charge neutralizer (2U500, NRD, NY, US). The SMPS system, which measures the mobility equivalent diameter, was operated at a sample flow of 0.3 l/min, a sheath flow of 3 l/min, and a scan time of 180 s (measurement range: 4.61–157 nm). The overall number, area, and mass concentration of the spark produced particles suspended in nitrogen gas were also measured using the SMPS system, both upstream and downstream from the substrates. The morphology and microstructure of the spark generated Ag nanoparticles were analyzed by high resolution transmission electron microscopy (HRTEM, JEM-3010, JEOL, Tokyo, Japan) operated at 300 kV. X-ray photoelectron spectroscopy (XPS) measurements of the activated substrates were performed using a Axis HIS spectrometer (Kratos Analytical, Manchester, UK) with a monochromatized Al Kα X-ray source (1486.6 eV photons). All binding energies (BEs) were referenced to the C1s hydrocarbon peak at 284.6 eV. Field-emission scanning electron microscope (FESEM, JSM-6500F, JEOL, Tokyo, Japan) images and energy dispersive X-ray (EDX, JED-2300, JEOL, Tokyo, Japan) profiles were obtained at an accelerating voltage of 15 kV. The amount of deposited Au on the substrates was determined by inductively coupled plasma atomic emission spectroscopy (ICPAES, Elan 6000, Perkin-Elmer, MA, US). Atomic force microscopy (AFM) was used for the topography of the electroless Au deposited substrate. Topographic images of the substrate were recorded under ambient conditions using a multimode scanning probe microscope (SPM) connected to a controller (NanoScope IIIa, Veeco, NY, US). The SPM was operated in tapping mode which allowed topography and phase contrast images to be recorded. The drive frequency was

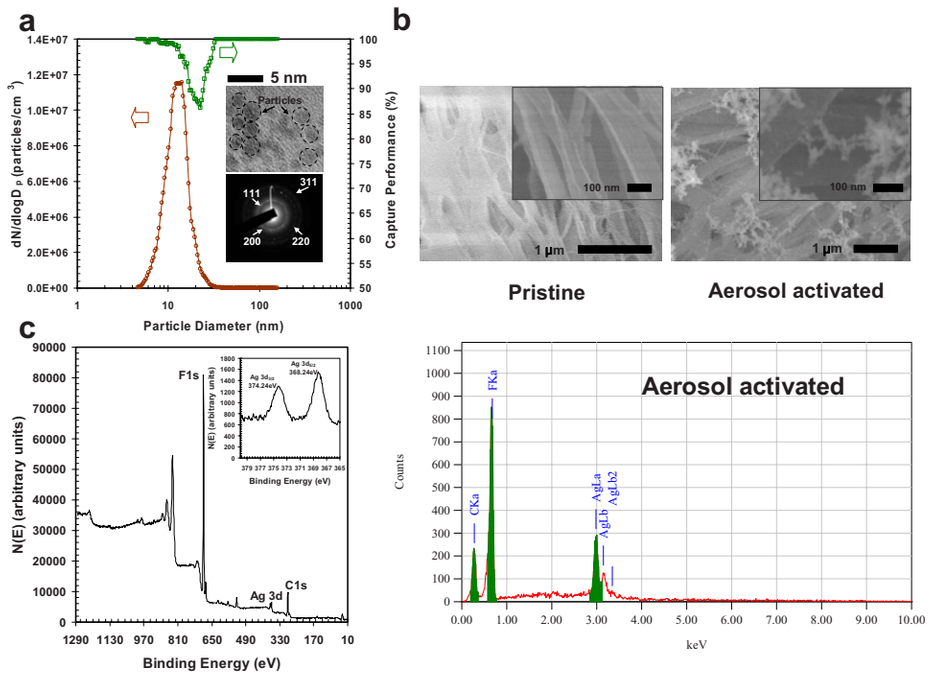

Figure 2. (Color online) Characterizations of the aerosol activation. (a) Particle size distribution and capture performance of the PTFE substrate, with (inset) the HRTEM micrograph and the ED pattern. (b) High- and low-magnitude FESEM micrographs and EDX spectra of pristine and aerosol activated substrates. (c) Wide and Ag 3d XPS profiles of the aerosol activated substrate.

330 kHz and the voltage ranged from 3.0 to 4.0 V. The drive amplitude was approximately 300 mV and the scan rate was 0.5–1.0 Hz. X-ray diffraction (XRD) studies of the deposited Au were carried out on a Rigaku RINT-2100 diffractometer equipped with a thin-film attachment using Cu-Kα radiation (40 kV, 40 mA). The 2θ angles ranged from 10 to 90° at 4°/min by step scanning at an interval of 0.08°.

Results and Discussion

Figure 2a shows the size distribution of the spark produced Ag aerosol nanoparticles which was obtained using the SMPS system. The geometric mean diameter and geometric standard deviation were 12.3 nm and 1.34, respectively. The overall number, area, and volume concentrations were 3.55×10^6 particles/cm^3, 2.01×10^9 nm^2/cm^3, and 5.18×10^9 nm^3/cm^3, respectively. Figure 2a also shows the fractional (grade) capture performance of the substrates as a function of the particle size which was calculated using the following equation

$$P(d_p) = 1 - \left[\frac{C_f(d_p)}{C_i(d_p)}\right] \quad [6]$$

where $C_i(d_p)$ is the freestream particle concentration and $C_f(d_p)$ is the concentration after capture by the substrate. The overall capture performance is defined as follows

$$P_{overall} = \frac{\int_0^\infty P(d_p)C_i(d_p)\mathrm{d}d_p}{\int_0^\infty C_i(d_p)\mathrm{d}d_p} \quad [7]$$

The Ag particle collection performance of substrate was 97.7% and indicated that a loss proportion of spark produced Ag particles was about 2% in number count. The HRTEM micrograph (inset of Fig. 2a) shows that single particle sizes of the spark produced nanoparticles were distributed around ~3 nm in diameter which suggested that the mean diameter from the SMPS analyses was for agglomerates. The electron diffraction pattern (inset of Fig. 2a) revealed characteristic rings in the polycrystalline diffraction pattern. Spacing was observed at 2.36, 2.04, 1.44, and 1.22 Å which were all within 2% of the value reported for the (111), (200), (220), and (311) face-centered cubic (fcc) Ag reflection [Joint Committee on Powder Diffraction Standards (JCPDS) no. 1-1167], respectively.

Figure 2b shows FESEM micrographs of the surfaces of the pristine and activated PTFE substrates with low and high (inset) magnifications. While the pristine PTFE had a clean surface, a number of spots were observed on the activated PTFE. The spots had a dendrite shape consisting of chains of small single particles (corresponding to HRTEM micrograph). EDX results (also shown in Fig. 2b) showed small peaks of Ag (the binding energies of 2.98 and 3.18 keV belonging to Ag $L_{\alpha 1}$ and Ag $L_{\beta 1}$, respectively) in the activated PTFE, but not on the pristine PTFE (not shown). It could be suggested that the dendrites were composed of Ag single particles. Carbon (C) and fluorine (F), which might have originated from the PTFE, were also detected.

The wide and Ag 3d (inset) XPS profiles (Fig. 2c) of the activated substrate showed that it contained Ag. The BE doublets (inset) of the Ag $3d_{3/2}$ and Ag $3d_{5/2}$ peak components located at approximately 368 and 374 eV, respectively, were assigned to Ag^0 species.[33] The wide XPS profile revealed significant peaks of C and F which corresponded to those in EDX. From the above results, a mass concentration (235.7 μg/m^3 for overall) of Ag nanoparticles can be estimated, and thus the activation intensity (I_a) [34] is defined as follows

$$I_a = \left[\int_0^\infty \eta(d_p)C_m(d_p)\mathrm{d}d_p\right]\left[\frac{Qt_a}{A_{sub}}\right] \quad [8]$$

where $C_m(d_p)$ is the mass concentration of Ag nanoparticles, Q is the flow rate of nitrogen gas, t_a is the activation time, and A_{sub} is the flat face area of substrate. The activation intensity was approximately 8.7 μg Ag/cm^2 PTFE.

Figure 3a shows that FESEM micrographs of the substrate surface after 60, 120, and 180 min immersion in Au ELD solution and morphologies of island films were similar to those as described by Blum et al.[42] Initially, small nodular particles with large island films were observed after 60 min of deposition. The size of the nodules increased to islands and an enlargement of the island films, already formed at 60 min of deposition, occurred after 120 min of deposition. When the deposition time increased to 180 min, a nearly uni-

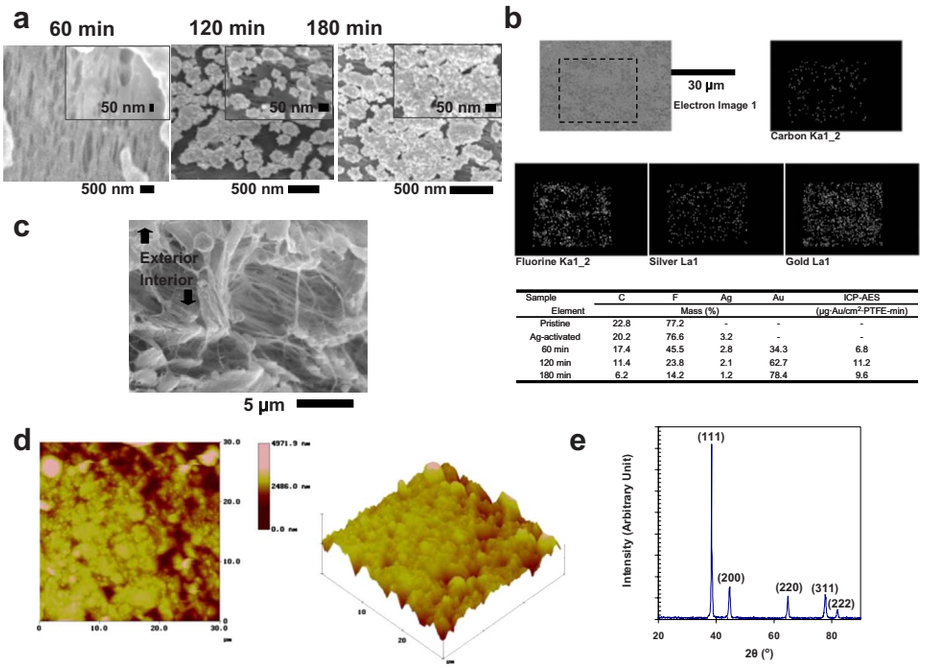

Sample	C	F	Ag	Au	ICP-AES
Element	Mass (%)				(µg Au/cm²-PTFE-min)
Pristine	22.8	77.2	-	-	-
Ag-activated	20.2	76.6	3.2	-	-
60 min	17.4	45.5	2.8	34.3	6.8
120 min	11.4	23.8	2.1	62.7	11.2
180 min	6.2	14.2	1.2	78.4	9.6

Figure 3. (Color online) Characterizations of Au ELD. (a) High- and low-magnitude FESEM micrographs of electroless film deposited substrates for ELD times of 60, 120, and 180 min. (c) Cross-section micrograph for 180 min of deposition. (b) EDX map results for 120 min of deposition. (d) 3D AFM image for 180 min of deposition. (e) The XRD pattern for 120 min of deposition.

form film was observed and most surfaces of the substrate were covered by the film. However, after 180 min of deposition, an island (discontinuous) film character was remained; some voids were still seen between and/or at the island films.

The first image in Fig. 3b shows a different scaled micrograph for 120 min of deposition. The following four images show the EDX maps of the dotted area in the first image. These maps corresponded to C, F, Ag, and Au, respectively. The dots in these images indicate the positions of each element in the first image. For example, Au was concentrated in the area corresponding to the white islands in the first image which shows that the islands on the substrate were Au. A corresponding spectrum (not shown) indicated that the binding energies of 1.66, 2.12, 2.21, and 9.71 keV belonged to Au M_{α}, Au $M_{\alpha 12}$, Au M_{β}, and Au $L_{\alpha 1}$, respectively, which were derived from the Au ELD. From the EDX compositions (see the table in Fig. 3b), it is found that the activated substrate contained C and F which might have originated from the substrate while a small amount of Ag also existed. The mass deposition rates of Au were obtained from the ICPAES analyses, and the rates for 60, 120, and 180 min of deposition were 6.8, 11.2, and 9.6 µg Au/cm^2 PTFE-min, respectively (see the table in Fig. 3b).

In looking at the distribution of island films with respect to each of the deposition times, two interesting phenomena were observed. First, after only 60 min of deposition, the surface of the substrate was covered with small nodular particles and large isolated island films. From this, it could be concluded that once displacement deposition has occurred at a site between Au and Ag,[25] then depositions by galvanic displacement and autocatalysis began to compete. These initial nucleation sites acted as autocatalysts for the oxidation of $H_2PO_2^-$ allowing for further Au deposition onto these sites. These initial nucleation sites continued to grow as separate islands until eventually the Au islands grew into one another.[43] The spacing between these initial nucleation sites, which was represented by the size of these islands after they have grown into one another, was termed the nucleation distribution distance. Consequently, pores on the surface of the substrate might have enhanced the formation of the spacing.

A cross-section micrograph (Fig. 3c) shows depth morphology of the Au deposited substrate for 180 min of deposition. From the micrograph, the Au deposits were rarely distributed on the interior surface rather than the exterior surface of the substrate and there seemed to be preferential nucleation sites for the Au deposition. Therefore, the morphology of the resulting Au deposits was different from other studies,[19-21,25] which synthesized cylindrically templated Au deposits using track-etch polymeric substrates. This might be due to the complexity of the inner structure of the substrate; a capture of the Ag aerosol particles was preferred at the exterior surface of the substrate during the activation.[44,45] As shown in Fig. 2b, the activation induced dendrites to form and then grew on the upstream side (exterior surface) rather than the interior surface of the substrate. These formations could have resulted from two related phenomena:[45] one is the shadowing effect and chain formation and the other is the random capture of individual Ag particles from the spark production. Moreover, an exterior surface Au dominated character was in direct correlation to the diffusion behavior exhibited by the Au^{3+} ions and was not uniform over the entire area of the interior structure of the substrate (refer to Fig. 1b); Au deposition only can be initiated on Ag particles. Moreover, the collection of aerosol particles using porous media normally dominated on exterior surface of the media owing to diffusion and interception phenomena [refer to Figs. 3c and 4 (the last one)].[46] Correspondingly, there was a higher deposition rate of Au on the exterior surface, resulting in thicker island films near the pores on the surface and a similar result was described in the study by Gilliam et al.[25]

Figure 3d shows the two-dimensional (left) and three-dimensional (right) AFM images of electrolessly deposited Au film for 180 min of deposition on the PTFE surface. The deposited Au film shows a periodic parallel and row-like structure. Many pellets in each row were clearly observed and had an average diameter ~1.6 µm, which was similar to the diameter (~2 µm) of the films in the previous 180 min micrograph in Fig. 3a, and they were organized in a two-dimensional pattern. Because of the discontinuity of the rows, the macrostructure of the Au film was more like an island growth. The thickness of the film was about 3.1 µm [the estimated lateral growth rate (film thickness per deposition time) was 17.2 nm/min].

Figure 3e shows sharp peaks at around $2\theta = 38.3$, 44.5, 64.8. 77.9, and 81.9° for 120 min of deposition. A comparison of these peaks with the data from the JCPDS file (no. 4-0784) revealed that these peaks corresponded to the (111), (200), (220), (311), and (222) planes of the fcc phase of Au; all the trimmings exhibited small

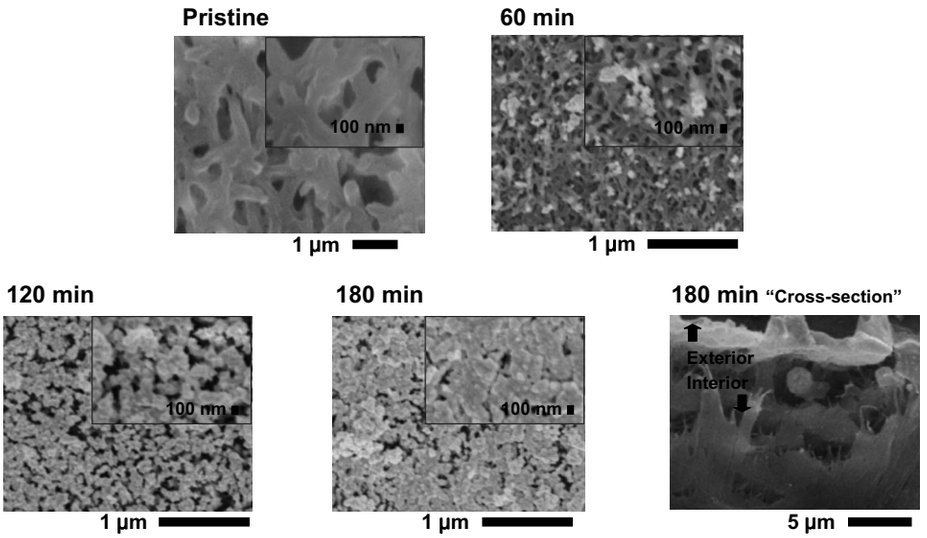

Figure 4. Growth pattern of Au films on the PA surface.

intensities compared to the Au (111) peak. The narrow (111) peak suggested that the crystallite size at the dominant orientation was large. The average crystallite sizes estimated from the XRD line broadening of the (111) peak, according to Scherrer's equation [$t = 0.9\lambda/(B \cos \theta)$], were 14, 41, and 62 nm for the 60, 120, and 180 min of deposition, respectively. The Au crystallite sizes were much smaller than the films in FESEM micrographs (Fig. 3a) which indicated that the Au films were polycrystalline.[24]

The Au deposition procedure was further conducted to a porous PA substrate. Even though the substrate had a different structure of the surface, the growth pattern of Au films during 180 min of deposition was similar to that of the PTFE with the exterior dominated by Au coverage of the substrate. However, a lateral mass growth rate (8.8 μg Au/cm^2 PA-min) was slightly different from that (9.6 μg Au/cm^2 PTFE-min) in PTFE probably due to a different activation intensity (7.9 μg Ag/cm^2 PA), which induced different values of crystallite size (11–60 nm) for 60–180 min of deposition. A difference of the activation intensity under the same activation operation between PTFE and PA substrates might be due to a capturing action of Ag particles with a substrate packing density (α) of diffusion and interception mechanisms, which can be estimated from the correlations[46]

$$P_D = 2.9\left(\frac{1-\alpha}{K_u}\right)^{1/3} P_e^{-2/3} \quad [9]$$

$$P_I = \frac{(1-\alpha)}{K_u}\frac{N_R^2}{(1+N_R)^m} \quad [10]$$

where P_D and P_I are the performances for diffusion and interception, respectively, K_u is the Kuwabara hydraulic factor ($K_u = -0.5 \ln \alpha - 0.75 + \alpha - 0.25\ \alpha^2$), P_e is the Peclet number, N_R is the interception parameter, and $m = 2/[3(1-\alpha)]$. Herein, the packing densities from different substrate structures (PTFE versus PA) might affect characteristics of discontinuous Ag deposit as island growth templates for ELD by Au. As shown in Fig. 1b, Au deposition could only be initiated on Ag particles, and therefore the different formation of Au island films on exterior surface of different substrates might be induced.

Conclusions

This paper describes a new strategy for fabricating a Au island film based on a Ag aerosol surface activation onto a porous PTFE substrate, followed by ELD. Spark produced Ag aerosol nanoparticles (~12.3 nm in diameter) were physically captured (8.7 μg Ag/cm^2 PTFE in activation intensity) onto the surface of the substrate. After annealing at 240°C, the activated substrate was placed into a solution for Au ELD at 90°C. Successive Au deposition introduced an island film having the thickness of ~3.1 μm (the lateral mass and dimensional growth rates of 9.2 μg Au/cm^2 PTFE-min and 17.2 nm/min, respectively), which was similar to the diameter of the island films at 180 min of deposition. X-ray diffraction certified the uniformity of the films with the Au (111) crystallographic orientation as the predominant one. The corresponding crystallite sizes ranged from 14 to 62 nm for 60–180 min of deposition. Island Au growth was also achieved using the present method for a different porous substrate (polyamide). Through these results, the Ag aerosol activation on a substrate with an uneven surface structure might preferably introduce an island electroless growth of Au. Our ELD for layering Au may be attractive for various scientific and/or engineering applications because the catalytic activation of the substrate is simple, inexpensive, and environmentally friendly and this can be favorably applied to interfacial applications ranging from self-assembled monolayers to sensing and heterogeneous catalysis.

Hoseo University assisted in meeting the publication costs of this article.

References

1. K. R. Brown and M. J. Natan, *Langmuir*, **14**, 726 (1998).
2. G. J. Hutchings, *Catal. Today*, **138**, 9 (2008).
3. L. Q. Nguyen, C. Salim, and H. Hinode, *Appl. Catal., A*, **347**, 94 (2008).
4. H. Chen, Y. Zheng, J.-H. Jiang, H.-L. Wu, G.-L. Shen, and R.-Q. Yu, *Biosens. Bioelectron.*, **24**, 684 (2008).
5. M. Mazur, A. Michota-Kamińska, and J. Bukowska, *Electrochim. Acta*, **52**, 5669 (2007).
6. M. A. Rafiq, H. Mizuta, S. Uno, and Z. A. K. Durrani, *Microelectron. Eng.*, **84**, 1515 (2007).
7. M. S. Raven, *Phys. Rev. B*, **29**, 6218 (1984).
8. K. Baba, J.-I. Katsu, and M. Miyagi, *Opt. Lett.*, **17**, 622 (1992).
9. C. Domingo, J. V. García, S. Sánchez-Cortés, and J. A. Aznarez, *J. Mol. Struct.*, **661–662**, 419 (2003).
10. R. D. Fedorovich, D. S. Inosov, O. E. Kiyaev, S. P. Lukyanets, A. A. Marchenko, P. M. Tomchuk, D. A. Bevzenko, and A. G. Naumovets, *J. Mol. Struct.*, **708**, 67 (2004).
11. S. Szunerits, V. G. Praig, M. Manesse, and R. Boukherroub, *Nanotechnology*, **19**, 195712 (2008).
12. R. D. Fedorovich, A. G. Naumovets, and P. M. Tomchuk, *Phys. Rep.*, **328**, 73 (2000).
13. W. Ahn, B. Taylor, A. G. Dall'Asén, and D. K. Roper, *Langmuir*, **24**, 4174 (2008).
14. C. Fukuhara, Y. Kamata, and A. Igarashi, *Appl. Catal., A*, **296**, 100 (2005).
15. T. Homma, I. Komatsu, A. Tamaki, H. Nakai, and T. Osaka, *Electrochim. Acta*, **47**, 47 (2001).
16. H. Miyake, S. Ye, and M. Osawa, *Electrochem. Commun.*, **4**, 973 (2002).
17. L. A. Porter, Jr., H. C. Choi, A. E. Ribbe, and J. M. Buriak, *Nano Lett.*, **2**, 1067 (2002).
18. S. Warren, A. Reitzle, A. Kazimirov, J. C. Ziegler, O. Bunk, L. X. Cao, F. U. Renner, D. M. Kolb, M. J. Bedzyk, and J. Zegenhagen, *Surf. Sci.*, **496**, 287 (2002).
19. V. P. Menon and C. R. Martin, *Anal. Chem.*, **67**, 1920 (1995).
20. M. Wirtz, S. Yu, and C. R. Martin, *Analyst (Cambridge, U.K.)*, **127**, 871 (2002).

21. J. C. Hulteen and C. R. Martin, *J. Mater. Chem.*, **7**, 1075 (1997).
22. A. Hilmi and J. H. T. Luong, *Anal. Chem.*, **72**, 4677 (2000).
23. Z. Hou, N. L. Abbott, and P. Stroeve, *Langmuir*, **14**, 3287 (1998).
24. Y. Kobayashi, Y. Tadaki, D. Nagao, and M. Konno, *J. Colloid Interface Sci.*, **283**, 601 (2005).
25. R. J. Gilliam, S. J. Thorpe, and D. W. Kirk, *J. Appl. Electrochem.*, **37**, 233 (2007).
26. S. Szunerits and D. R. Walt, *Anal. Chem.*, **74**, 1718 (2002).
27. T. B. Dubrovsky, Z. Hou, P. Stroeve, and N. L. Abbott, *Anal. Chem.*, **71**, 327 (1999).
28. A. A. Mewe, E. S. Kooij, and B. Poelsema, *Langmuir*, **22**, 5584 (2006).
29. S. Hrapovic, Y. Liu, G. Enright, F. Bensebaa, and J. H. T. Luong, *Langmuir*, **19**, 3958 (2003).
30. M. Kato, J. Sato, H. Otani, T. Homma, Y. Okinaka, T. Osaka, and O. Yoshioka, *J. Electrochem. Soc.*, **149**, C164 (2002).
31. T. Osaka, T. Misato, J. Sato, H. Akiya, T. Homma, M. Kato, Y. Okinaka, and O. Yoshioka, *J. Electrochem. Soc.*, **147**, 1059 (2000).
32. T. Osaka, Y. Okinaka, J. Sasano, and M. Kato, *Sci. Technol. Adv. Mater.*, **7**, 425 (2006).
33. F. Jing, H. Tong, L. Kong, and C. Wang, *Appl. Phys. A*, **80**, 597 (2005).
34. J. H. Byeon, B. J. Ko, and J. Hwang, *J. Phys. Chem. C*, **112**, 3627 (2008).
35. J. H. Byeon, J. H. Park, K. Y. Yoon, and J. Hwang, *Langmuir*, **24**, 5949 (2008).
36. J. H. Byeon, K. Y. Yoon, Y. K. Jung, and J. Hwang, *Electrochem. Commun.*, **10**, 1272 (2008).
37. J. H. Byeon, J. H. Park, and J. Hwang, *J. Aerosol Sci.*, **39**, 888 (2008).
38. K. Ostrikov and A. B. Murphy, *J. Phys. D: Appl. Phys.*, **40**, 2223 (2007).
39. M. Keidar, I. Levchenko, T. Arbel, M. Alexander, A. M. Waas, and K. Ostrikov, *Appl. Phys. Lett.*, **92**, 043129 (2008).
40. J. Chen, G. Lu, L. Zhu, and R. C. Flagan, *J. Nanopart. Res.*, **9**, 203 (2007).
41. J. H. Byeon, J. H. Park, K. Y. Yoon, and J. Hwang, *Nanoscale*, 1, 339 (2009).
42. B. Blum, R. C. Salvarezza, and A. J. Arvia, *J. Vac. Sci. Technol. B*, **17**, 2431 (1999).
43. Y. Y. Shacham-Diamand, *Electrochem. Solid-State Lett.*, **3**, 279 (2000).
44. V. A. Kirsch, *Sep. Purif. Technol.*, **58**, 288 (2007).
45. B. Huang, Q. Yao, S.-Q. Li, H.-L. Zhao, Q. Song, and C.-F. You, *Powder Technol.*, **163**, 125 (2006).
46. A. Bałazy and A. Podgórski, *J. Colloid Interface Sci.*, **311**, 323 (2007).